

(NASA-CR-120736) WORKING MODEL OF THE  
LONDON MOMENT READOUT SYSTEM Semiannual  
Progress Report, 1 Jan. - 30 Jun. 1974  
(Alabama Univ., Huntsville.) 38 p HC \$3.75

N75-21562

Unclas  
CSCL 13K G3/34 19247

WORKING MODEL  
OF THE  
LONDON MOMENT READOUT SYSTEM

January 1, 1974 - June 30, 1974

John Benjamin Hendricks  
and  
Gerald R. Karr

The University of Alabama in Huntsville  
School of Graduate Studies and Research  
Huntsville, Alabama 35807

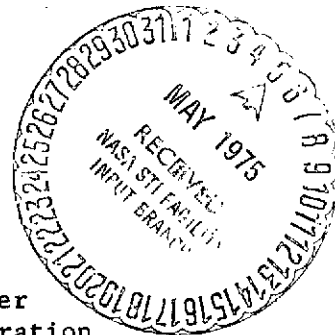
SEMI-ANNUAL PROGRESS REPORT

Contract Number NAS8-29316

Prepared for

George C. Marshall Space Flight Center  
National Aeronautics and Space Administration  
Marshall Space Flight Center, Alabama 35812

March 1975



## I. PROGRESS ON STUDY PROGRAM

This progress report covers the work done by Dr. Karr on the theory of super fluid plug operation. The purpose of the work was to develop expressions which explain the behavior of the super fluid plug which is being proposed for use in liquid helium management in space for the relativity experiment.

The details of the calculations and results are provided in the appendix. In summary, the essential results are that the mass flow rate,  $\dot{m}$ , through the plug is given by the expression

$$\frac{\dot{m}}{A_T} = \frac{P_v(T) + P_h}{\frac{\rho S L \ell}{K} + \left( \frac{1}{\left( \frac{FA}{A_T} \right)^*} \right)}$$

where  $A_T$  is the total area of the plug,  $\rho$  is the density,  $S$  is the entropy,  $L$  is the latent heat of vaporization, and  $K$  is the total thermal conductivity of the plug with the liquid helium included. All properties are for the helium in the liquid state evaluated at the temperature on the liquid side of the plug. The factor  $\frac{FA}{A_T}^*$  is related to the impedance of the pumping system on the gas side of the plug.

Solution was also obtained for the mass flow at temperature above the lambda point temperature given by

$$\frac{\dot{m}}{A_T} = \frac{P_v(T) + P_h}{\frac{\mu \ell A_T}{\rho k A_p} + \left( \frac{1}{\left( \frac{FA}{A_T} \right)^*} \right)}$$

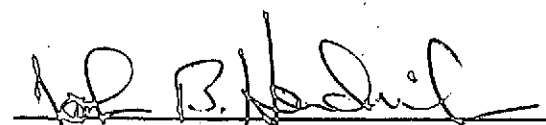
where  $\mu$  is the viscosity,  $k$  is the permeability of the plug and  $A_p$  is the total area of pores contained in a cross section of the plug. The value of  $A_p$  is found from measurement of the plug porosity.

Solutions were obtained for the normal and superfluid velocity (equation 29 and 30 of the appendix). This was done in order to investigate the possibility of the superfluid component reaching the critical velocity, thereby violating certain assumptions in the derivation. We found that for the plugs of pore sizes under consideration here, that the superfluid velocity is always less than the critical velocity. We also conclude that only for pore sizes larger than 10 micron would this effect become of importance.

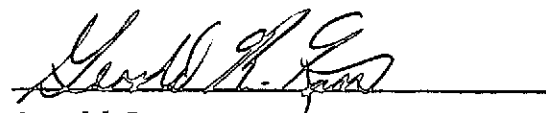
A brief comparison of the theory results with the experimental results obtained by Dr. Urban are made. We find that the theory is very accurate in the region of 1.5°K but departs as much as 30% at near 2°K. The source of error is believed to be the approximate linear relationship used to represent the pumping system impedance.

## II. PLANS FOR NEXT REPORTING PERIOD

The next semi-annual progress report will cover work on the magnetometer and low temperature research apparatus by Dr. Hendricks and work on magnetic shielding calculations.



John B. Hendricks  
Principal Investigator



Gerald R. Karr  
Principal Investigator

asw

## APPENDIX

## THEORY OF SUPER FLUID PLUG OPERATION

by

Gerald R. Karr

## I. INTRODUCTION

The operating characteristics of a porous plug which has liquid helium on one side and which is pumped on under vacuum on the other side is discussed. Such a device has application to the containment of liquid helium in a zero gravity environment. The plug has the capability of acting as a phase separator and, to some extent, as a temperature control device.

The system to be considered in the work consists of a container of liquid helium which is well isolated. The only means for mass flow out of the container is through a plug made of porous material. The plug is assumed to have liquid helium on the container side while the other side of the plug is evacuated. In the experiment ran on earth under one g, the plug is situated on the bottom of the container. The physical system employed in the evacuation is found to be important to the plug operation. Three cases in particular will be considered: (1) perfect evacuation with zero pressure, (2) evacuation through an choked orifice, and (3) evacuation through a long, small diameter pipe with heating. The last case is the one most likely to occur in practice.

Two distinct ranges of temperature operation are of importance in describing plug flow. (1) Above  $T = 2.172^{\circ}\text{K}$  and (2) Below  $T = 2.172^{\circ}\text{K}$ . The temperature  $2.172^{\circ}\text{K}$  is the point at which liquid helium changes from HeI which exists at the higher temperature range to a second liquid

phase HeII at the lower range of temperature. HeI is a normal liquid phase and the flow of this liquid is described by classical fluid flow relationships. In the HeII phase, however, the fluid exhibits super fluid properties which must be taken into consideration.

For purposes of describing the plug operation, the two-fluid model of the HeII phase is used. The two-fluid model considers HeII to consist of a super fluid component,  $\rho_s$ , and a normal fluid component,  $\rho_n$ , where the total density of the fluid,  $\rho$ , is given by

$$\rho = \rho_s + \rho_n$$

The ratio  $\rho_n/\rho$  drops from a value of one at the  $\lambda$ -point and asymptotically approaches zero at  $0^\circ\text{K}$ .

The fluid flow of HeII using the two-fluid model is described by the following set of Landau's equations (see for example R. J. Donnelly, Experimental Superfluidity, University of Chicago Press, 1967),

$$\rho_s \frac{\partial \vec{v}_s}{\partial t} + \rho_s (\vec{v}_s \cdot \nabla) \vec{v}_s = - \frac{\rho_s}{\rho} \nabla p + \rho_s S \nabla T + \frac{\rho_n \rho_s}{\partial \rho} \nabla (\vec{v}_n - \vec{v}_s)^2 \quad (1)$$

$$\begin{aligned} \rho_n \frac{\partial \vec{v}_n}{\partial t} + \rho_n (\vec{v}_n \cdot \nabla) \vec{v}_n = & - \frac{\rho_n}{\rho} \nabla p - \rho_s S \nabla T \\ & - \frac{\rho_n \rho_s}{\partial \rho} \nabla (\vec{v}_n - \vec{v}_s)^2 + \mu \nabla^2 \vec{v}_n \end{aligned} \quad (2)$$

The first term on the right hand side represents the reaction of the fluid to pressure forces, the second term is associated with the thermo-mechanical effect, and the third term is a mutual friction dependent on

the motion of one component with respect to the other. Equation (2) contains a fourth term on the right hand side which represents the effect of viscosity. The flow equation for temperature above the  $\lambda$  point can be obtained from equation (2) for the case of  $\rho_s = 0$  and  $\rho_n = \rho$ .

The flow equations are found to reduce considerably for the combination of steady state flow and small  $\nabla T$  across the plug. These conditions are reasonable assumptions for plugs made with large pore (5-10 $\mu$ ) material. For small pore material (.5 $\mu$ ), the  $\nabla T$  across the plug is found to be large. Also, small pore materials seem to exhibit time dependent behavior which may require non-steady state analysis.

In summary, the description of porous plug operation for liquid helium management is divided into the following items of importance.

1. Type of evacuation
  - a. perfect vacuum
  - b. through orifice
  - c. through pipe with heating
2. Temperature range
  - a. above  $\lambda$ -point
  - b. below  $\lambda$ -point
3. Simplifying assumptions
  - a. steady state
  - b. small  $\nabla T$
4. Velocity range of superfluid
  - a. less than critical velocity
  - b. greater than critical velocity

This report will consider the special case of small  $\nabla T$ , steady state operation of a plug evacuated through an ideal orifice over the full temperature range. The results will be reducible to the case of a perfect vacuum evacuation. Future progress reports will consider the case of evacuation through a pipe with heating and large  $\nabla T$  across the plug.

## II. SMALL $\nabla T$ WITH EVACUATION THROUGH CHOKED ORIFICE

The model of the system to be described is shown in Figure 1. The flow through the orifice is linear in the pressure difference across the orifice. If the pressure downstream of the orifice is small compared to the pressure in the plenum,  $P_p$ , the mass flow per unit area through the orifice is given by

$$\dot{m}/A^* = F P_p \quad (3)$$

where  $\dot{m}$  is the mass flow rate,  $A^*$  is a flow area at the point that Mach Number  $M=1$ , and  $F$  is given for a choked orifice by

$$F = C_w \sqrt{\frac{\gamma}{RT_p} \frac{2}{\gamma+1} \frac{\gamma+1}{\gamma-1}} \quad (4)$$

where  $C_w$  is a orifice discharge coefficient,  $\gamma$  is the ratio of specific heats,  $R$  is the gas constant of the gas and  $T_p$  is the temperature of the gas in the plenum. For pressure ratios across the orifice of .1 or less, the value of  $C_w$  is 0.85.

In normal operation, heat is transferred out of the container through the plug at a rate proportional to the conductivity across the plug. The heat comes from heat leaks into the container due to imperfect



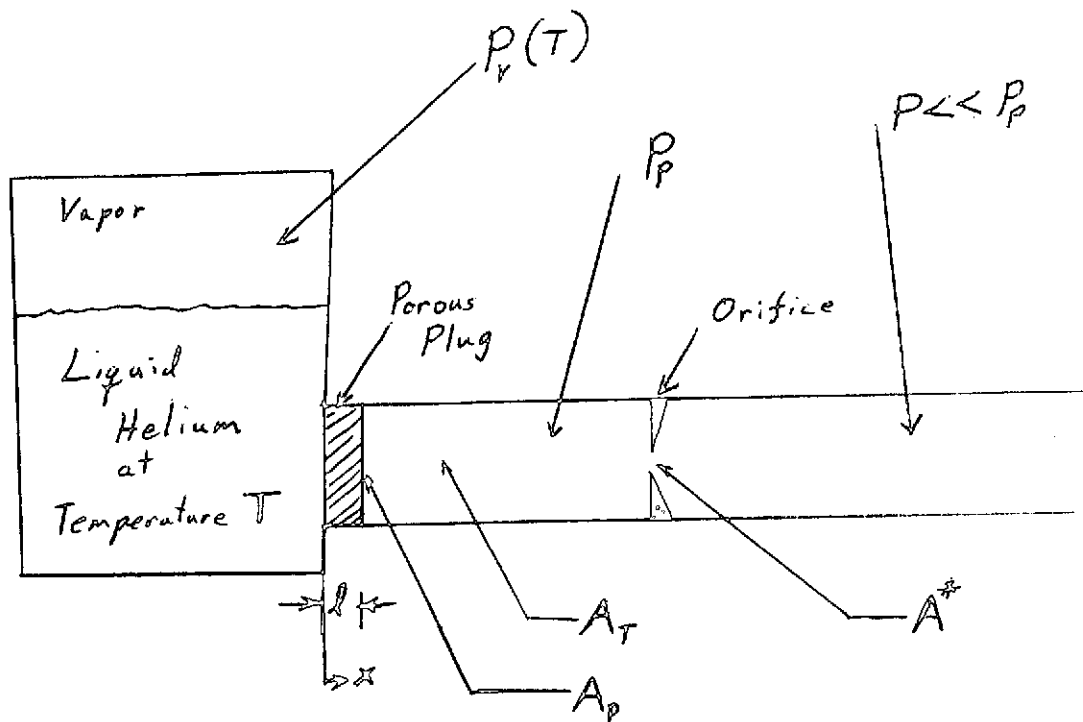


FIGURE 1: Model of Super Fluid Plug System Considered in Analysis

ORIGINAL PAGE IS  
OF POOR QUALITY

isolation or from heat given off by experimental equipment inside the container.

An analytic solution to equations (1) and (2) is obtained for the case of choked orifice and certain assumptions concerning the liquid flow in the plug. One simplification becomes apparent if equation (1) is added to equation (2). The result is

$$\begin{aligned} \rho_s \frac{\partial \vec{v}_s}{\partial t} + \rho_n \frac{\partial \vec{v}_n}{\partial t} + \rho_s (\vec{v}_s \cdot \nabla) \vec{v}_s + \rho_n (\vec{v}_n \cdot \nabla) \vec{v}_n \\ = - \nabla p + \mu \nabla^2 \vec{v}_n \end{aligned} \quad (5)$$

The right hand side of Equation (5) is the incompressible, steady-state Navier-Stokes equation for parallel flow. Parallel flow means that the flow has components in one direction only. If the left hand side of equation (5) can be neglected, the problem is greatly simplified. The first two terms of equation (5) are zero for steady-state conditions. The third and fourth terms are zero for the case of parallel flow and small temperature drop (based on continuity). The assumptions of parallel flow is justified even for flow in a porous material if one considers averages over regions that are large compared to the pore size. The continuity equation for the two-fluid model and parallel flow is

$$v_s \frac{\partial \rho_s}{\partial x} + \rho_s \frac{\partial v_s}{\partial x} + v_n \frac{\partial \rho_n}{\partial x} + \rho_n \frac{\partial v_n}{\partial x} = 0 \quad (6)$$

Although the flow is considered incompressible,

$$\rho_n + \rho_s = \text{constant} \quad (7)$$

the individual densities are a strong function of temperature as discussed earlier. For this reason, the derivatives of  $\rho_g$  and  $\rho_n$  may be finite if a temperature gradient exists. Since heat transfer is taking place, one can neglect these derivatives only if the temperature gradient is small enough to make the resultant density gradient negligible. This condition can be met for plugs with large pores except near  $T_\lambda$  where the density changes are large with respect to temperature. The large pore plugs have a high effective thermal conductivity and therefore a small gradient of temperature as will be discussed later.

Under the assumption of small  $\Delta T$  and parallel flow, equation (5) becomes

$$\nabla p = \mu \nabla^2 \vec{v}_n \quad (8)$$

where the velocity  $\vec{v}_n$  is determined completely by the pressure drop. If the plug were constructed of smooth channels, such as a bundle of capillary tubes of radius  $R$ , the exact solution to the above for laminar pipe flow could be employed to find the volume flow rate given by

$$Q_n = \frac{2\pi R^4}{8\mu} - \left( \frac{dp}{dx} \right) \quad (9)$$

which shows that the flow rate is a linear function of the pressure drop. The plugs being considered by NASA at this time, however, are made of packed granular material which cannot be considered to have smooth passages.

For flow through porous material, a relationship similar to equation (9) is available given by Darcy's law (see Muskat, Flow of Homogeneous Fluids) .

$$v_n = - \frac{k}{\mu} \frac{dp}{dx} \quad (10)$$

where  $k$  is called the permeability of the porous material. Values of  $k$  must generally be determined experimentally since reliable theory has not been developed for the irregularly shaped granules contained in most porous substances. A good approximation, however, can often be made by use of Kozeny's equation

$$k = \frac{1}{5} \frac{p^3}{(1-p)^2 s^2} \quad (11)$$

where  $p$  is the fractional porosity and  $s$  is the total surface area of the particles contained in a unit volume of the medium. Fractional porosity is defined as the fractional volume of voids per unit total volume. This can be obtained by weighing a sample made of granules of known density. The value of  $s$  is related to the size of the granules which varies considerably in most materials.

The important result to this point is that the normal fluid velocity is a function of the pressure drop as given in equation (10). For the experimental apparatus under consideration, the pressure on the liquid side of plug is the vapor pressure associated with the temperature of the liquid. The liquid head above the plug will also contribute to the pressure. The pressure drop across the plug is then given by

$$-\Delta p = P_v(T) + P_h - P_p \quad (12)$$

where  $P_v(T)$  is the vapor pressure at temperature  $T$ ,  $P_h$  is the head pressure and  $P_p$  is the plenum pressure on the downstream side of the

plug. The pressure  $P_p$  is given as a function of mass flow rate in equation (3).

Considering the mass flow rate at the plug which is given by

$$\frac{\dot{m}}{A_p} = \rho_s v_s + \rho_n v_n \quad (13)$$

where  $A_p$  is the area of pores available for flow of liquid in the plug and the densities are for the liquid state. Equation (3) then becomes

$$\rho_s v_s + \rho_n v_n = F P_p \quad (14)$$

and, since

$$\dot{m} = F A^* P_p$$

then

$$P_p = \frac{A_p}{A^* F} (\rho_s v_s + \rho_n v_n) \quad (14a)$$

Letting  $\ell$  be the length of the plug,  $dp/dx$  can be written as  $\Delta p / \ell$ .

Equation 10 can now be written, using equation (12) and (14a)

$$v_n = \frac{k}{\mu \ell} \left[ P_v(T) + P_h - \frac{A_p}{A^* F} (\rho_s v_s + \rho_n v_n) \right] \quad (15)$$

which provides a relationship between  $\rho_s v_s$  and  $\rho_n v_n$  which will be used later.

In order to be consistent with the assumptions of parallel flow and small temperature gradient as used previously, Equation (1) should be written with the left hand side zero and the last term on the right hand side also neglected. Therefore, equation (1) becomes

$$\frac{\rho_s}{\rho} \nabla P = \rho_s S \nabla T$$

or

$$\nabla P = \rho S \nabla T \quad (16)$$

The gradient of  $T$  required in equation 16 is a function of temperature range (i.e., above or below  $T_\lambda$ ), the plug material, and the pore size as will be discussed.

Heat is transferred across the plug in proportion to the temperature drop and the thermal conductivity of the plug given by

$$\frac{q}{A_T} = K \nabla T \quad (17)$$

where  $A_T$  is the total area of the plug and where  $K$  is the thermal conductivity of the plug which has contributions from both the liquid  $K_L$ , and the solid materials,  $K_m$ , given by

$$K = K_m \frac{A_m}{A_T} + K_L \frac{A_L}{A_T} \quad (18)$$

where  $A_m$  and  $A_L$  are the respective areas of the two materials. Values of  $K_m$  as a function of temperature are available in the literature.

Donnelly discusses the effective thermal conductivity of liquid helium below  $T_\lambda$ . Since entropy can only be transported by the normal fluid component, the flow of heat then is restricted if the normal fluid flow is restricted. For the small openings that are encountered in porous materials, viscous effects strongly influence the flow of the normal fluid. Therefore, the smaller the flow spacing, the smaller the thermal conductivity. Donnelly gives as a result, for below  $T_\lambda$

$$K_L = \frac{\rho^2 S^2 T d^2}{12\mu} \quad (19)$$

where  $S$  is the entropy. Since  $S$  is a strong function of temperature,  $K_L$ , also becomes a strong function of temperature as evidenced by the approximation

$$K_L \approx 1.2 \times 10^5 T^{12.2} d^2 \quad (20)$$

Heat conductivity of helium at 3.3°k is only

$$K_L (3.3^\circ \text{k}) = 6 \times 10^5 \text{ cal/deg/cm/sec} \quad (21)$$

Large pore size then results in extremely high thermal conductivities below  $T_\lambda$  which tends to be the dominant term in equation 18.

The heat that is transferred across the plug is liberated in transforming the liquid into a gas at the surface of the plug. The heat flow then is related to the mass flow rate and the latent heat of vaporization,  $L$ , of the helium given by

$$\frac{q}{A_T} = L \frac{\dot{m}}{A_T} \quad (22)$$

Equating the heat flow expression from equation (17) and (22), we obtain

$$K \nabla T = L \frac{\dot{m}}{A_T} \quad (23)$$

Substituting for  $\nabla T$  in equation (16) using the above we get

$$\nabla P = \rho S \left( \frac{L}{K} \frac{\dot{m}}{A_T} \right) \quad (24)$$

Using equation (12) and (13), and (14) in equation (24)

$$\frac{P_v(T) + P_h - \frac{1}{F} (\rho_s v_s + \rho_n v_n) \frac{A_p}{A^*}}{\ell} = \rho S \frac{L}{K} (\rho_s v_s + \rho_n v_n) \frac{A_p}{A_T} \quad (25)$$

This equation is solved for  $\dot{m}$  directly

$$\frac{\dot{m}}{A_T} = \frac{P_v(T) + P_h}{\frac{\rho S L \ell}{K} + \left( \frac{1}{F A^*} \right) \left( \frac{A_p}{A_T} \right)} \quad (26)$$

Equation (26) gives the flow rate through the plug as a function of temperature of the liquid helium. These results are not the same as obtained by Selzer, Fairbank, and Everett given by

$$\dot{m} = \frac{\Delta P K}{\rho S L} \quad (27)$$

Equation (26) is seen to reduce to equation (27) for the special case of  $1/F = 0$  which corresponds to the case of zero pressure on the downstream side of the plug. Zero pressure is, however, an unrealistic assumption for laboratory systems. (A factor of length,  $\ell/A$ , is evidently missing from equation (27)).

#### CRITICAL VELOCITY LIMITING

Equation (26) applies only for superfluid velocities below the critical velocity. In order to assess the validity of this solution, the superfluid velocity,  $v_s$ , must be obtained to compare with the critical velocity,  $v_c$ . If the critical velocity is reached, another method of solution must be employed.

In order to obtain a solution for  $v_s$  and  $v_n$ , equations (26) and equation (15) are solved simultaneously. Substituting for  $\dot{m}/A_T$  from



equation (26) into equation (15), we get

$$v_n = \frac{k}{\mu \ell} \left[ 1 - \frac{1}{\frac{\rho S L \ell}{K} \left( \frac{FA^*}{A_T} \right) + 1} \right] (P_v(T) + P_h) \quad (28)$$

which gives the solution for  $v_n$ . This equation can be rewritten in a form similar to equation (26)

$$v_n = \frac{\frac{\rho S L k}{\mu K}}{\frac{\rho S L \ell}{K} + \left( \frac{1}{\left( \frac{FA^*}{A_T} \right)} \right)} (P_v(T) + P_h) \quad (29)$$

the velocity of the super fluid component is obtained using equation (29) with equation (26). The result is

$$v_s = \frac{\frac{A_T}{A_p} \frac{1}{\rho_s} \left( 1 - \frac{\rho_n \rho k S L A_p}{K \mu A_T} \right)}{\left[ \frac{\rho S L \ell}{K} + \frac{1}{\left( \frac{FA^*}{A_T} \right)} \right]} (P_v(T) + P_h) \quad (30)$$

The normal velocity is seen to always be a positive number while  $v_s$  may become negative if

$$\frac{\rho_n \rho k S L A_p}{K \mu A_T} > 1 \quad (31)$$

If the superfluid flow velocity should become greater than the critical velocity, equation 1 must be modified to include a viscous type term in the superfluid component. A solution for this case has not as yet been

developed since it was found that for the pore sizes and pressures under consideration, critical velocity was not reached. Critical velocity would be expected to become important, however, for larger sizes of pores and much higher pressure heads.

#### ABOVE $T_\lambda$

The flow rate above the transition temperature consists of only the normal fluid which is governed by Darcy's law as mentioned earlier. The flow is still effected by the orifice, however. Equation (12) for the pressure drop remains the same and equation (14) becomes, for flow of vapor,

$$F P_p = \frac{\dot{m}}{A^*} \quad (32)$$

Using equation (10) and (12) with the above we get

$$P_p = \frac{A_p}{A^* F} (\rho v)$$

$$v = \frac{k}{\mu \ell} (P_v(T) + P_h - \frac{A_p \rho}{A^* F} v) \quad (33)$$

where  $\rho$  is the density of the liquid helium.

Solving for  $\rho v$ , the flow above  $T_\lambda$  is given by

#### Above $T_\lambda$ results

$$\frac{\dot{m}}{A_T} = \frac{P_v(T) + P_h}{\frac{\mu \ell A_T}{\rho k A_p} + \left( \frac{1}{F A^*} \right)} \quad (34)$$

# SUMMARY OF BELOW $T_\lambda$ RESULTS

Below  $T_\lambda$

$$\frac{A_p}{A_T} (\rho_s v_s + \rho_n v_n) = \frac{\dot{m}}{A_T} = \frac{P_v(T) + P_h}{\frac{\rho S L \ell}{K} + \frac{1}{\left(\frac{FA^*}{A_T}\right)}} \quad (26)$$

where

$$v_n = \frac{\frac{\rho S L \ell k}{\mu K}}{\frac{\rho S L \ell}{K} + \frac{1}{\left(\frac{FA^*}{A_T}\right)}} (P_v(T) + P_h) \quad (29)$$

and

$$v_s = \frac{\frac{A_T}{A_p} \frac{1}{\rho_s} \left(1 - \frac{\rho_n \rho k S L A_p}{K \mu A_T}\right)}{\frac{\rho S L \ell}{K} + \frac{1}{\left(\frac{FA^*}{A_T}\right)}} (P_v(T) + P_h) \quad (30)$$

### Comparison with Experiment

The equations given above were evaluated over the temperature range of interest ( $1 \cdot K$  to  $T_\lambda$ ) for a number of plug parameters. The parameters associated with plugs being tested by Dr. Urban at MSFC were employed in the analysis and the comparison of these analytic results with the experimental results is presented here. The purpose of this discussion is to also describe the methods used to obtain some of the important parameters needed in the calculation. Some of the basic properties of a few of the plugs to be tested by Dr. Urban are given in Table I.

Table I

Material	Thickness, $\ell$	Diameter*	Porosity, P	Labeled Pore Diameter
Nickel	.00630 m	.04515 m	.384	10 micron
Stainless Steel	.00630 m	.04510 m	.311	10 micron
Copper	.00645 m	.04520 m	.467	10 micron
Ceramic	.00660 m	.04525 m	.677	10 micron
Ceramic	.00650 m	.04523 m	.548	.5 micron

\*The diameters listed are for the unmounted plug. The effective diameter of the plug in the holder is the same for all the plugs tested and is 0.0437 m.

### Porosity Determination

The values of porosity listed in Table I were arrived at by weighing the plug on a balance to obtain the bulk density,  $\rho_b$ , of the plug given by

$$\rho_b = \frac{\text{mass}}{\pi r^2 \ell} \quad (35)$$

The porosity of the plug is then found using the density of the material,  $\rho_m$ , in the following equation

$$P = 1 - \frac{\rho_b}{\rho_m} \quad (36)$$

The densities employed in determining the porosity were approximate values given in Table II.

Table II: Density of Plug Materials

Material	$\rho_m$ (gm/cm <sup>3</sup> )
Nickel	8.902
Stainless Steel	7.9
Copper	8.96
Ceramic, Al <sub>2</sub> O <sub>3</sub>	3.965

#### Permeability Determination

The permeability of the porous plugs were determined in Helium gas flow tests ran at room temperature by Dr. Katz. The tests consisted of measuring the time for the plug to pass a measured volume of Helium gas for a measured pressure drop across the plug. The results revealed a linear relationship between volume of gas per unit time versus pressure drop over a range of pressure drops from 1/2 to 4 psi. The results of these measurements are given in Table III.

Table III: Flow Rate Per Unit Pressure Drop

Material	Pore Size	$\Delta F/\Delta P$
Nickel	10 Micron	31.45 scc/sec/psi
Ceramic	10 Micron	18.64 scc/sec/psi
Ceramic	.5 Micron	0.448 scc/sec/psi
Ceramic	3 Micron	6.23 scc/sec/psi

The permeability of the plug is defined using Equation 10

$$k = \frac{v \mu}{dp/dx} \quad (37)$$

Since the flow experiment measures volume flow rate rather than the velocity called for in Equation 37, multiply the right hand side by  $A_T/A_T$  to obtain

$$k = \left( \frac{v A_T}{d p} \right) \frac{\mu dx}{A_T} \quad (38)$$

where the term in the bracket corresponds to the measurements given in Table III. Taking  $dx$  to be the plug length (see Table I), the area to be based on a diameter of 0.0437 m (see note with Table I), and the viscosity of the helium gas to be

$$\mu = 1.953 \times 10^{-5} \text{ n} \cdot \text{sec/m}^2$$

the permeability values obtained are given in Table IV.

Table IV: Permeability Values

Material	Pore Size	Permeability, $k$
Nickel	10 micron	$3.7716 \times 10^{-13} \text{ m}^2$
Ceramic	10 micron	$2.2354 \times 10^{-13} \text{ m}^2$
Ceramic	.5 micron	$5.3726 \times 10^{-15} \text{ m}^2$

### Effective Orifice Parameter

Equation 3 is a linear relationship between the flow rate and the back pressure developed on the gas side of the plug. This relationship is strictly valid only for a sharp edged orifice. The pumping line employed in the experimental apparatus to be considered here has a minimum diameter of 1/4 inch with many turns and a length of over six feet before expanding to a larger diameter. The pumping line reaches room temperature soon after leaving the dewar.

The restriction to the gas flow caused by the small diameter, long tube with high heating is represented in this analysis as a single sharp edged orifice. Modeling the pumping line restriction as a sharp edged orifice is not particularly accurate but serves to represent an important part of the plug system in a simple manner. Future work will incorporate a more accurate representation of the pumping line restriction which calls for an equation of the form,

$$\dot{m} = G P_P^2 \quad (39)$$

instead of the linear relationship given in Equation 3. The F factor in Equation 3 is a function of temperature on the gas side of the plug as given in Equation 4. This temperature dependence will be ignored in the present treatment since the error committed is less than the error of using Equation 3 rather than Equation 39.

The determination of F and  $A^*$  cannot be made separately but an effective orifice parameter can be found by writing Equation 3 as

$$\dot{m}/A_T = \left( \frac{FA^*}{A_T} \right) P_P \quad (40)$$

In Equation 40, the values of  $\dot{m}$ ,  $A_T$  and  $P_P$  are measurable quantities allowing the determination of the effective orifice parameter, placed in brackets in Equation 40. In one of the first plug experiments at MSFC, the values of  $\dot{m}$ ,  $A_T$  and  $P_P$  were monitored in order to obtain a value of  $FA^* / A_T$ . From these measurements the following value was obtained

$$\frac{FA^*}{A_T} = 1.0412 \times 10^{-6} \frac{\text{Kg}}{\text{m} \cdot \text{sec}} \quad (41)$$

which is representative of the pumping line restriction at temperature near 1.6 °K where the pumping rate was found to be near 500 scc/min.

#### Liquid Helium Properties

The following liquid helium properties are required for the computation of plug flow rates.

$P_V$	=	Vapor pressure
$S$	=	Entropy
$L$	=	Lantent heat of vaporization
$\rho_n$	=	Density of normal fluid component
$\rho_s$	=	Density of super fluid component
$\rho$	=	Total density of fluid = $\rho_s + \rho_n$
$\mu$	=	Viscosity of the normal fluid component

The vapor pressure is obtained from a curve fit relationship provided by NBS which gives the vapor pressure in units of  $\text{n/m}^2$

$$P_V = 1.33322 \times 10^5 \text{ EXP } a_1 T + a_2 + a_3/T + a_4/T^2 + \dots + a_{14}/T^{12} \quad (42)$$



where

$$\begin{aligned}
 a_1 &= -49.510540356 \\
 a_2 &= 651.92364170 \\
 a_3 &= -3707.5430856 \\
 a_4 &= 12,880.673491 \\
 a_5 &= -30,048.545554 \\
 a_6 &= 49,532.267436 \\
 a_7 &= -59,337.558548 \\
 a_8 &= 52,311.296025 \\
 a_9 &= -33,950.233134 \\
 a_{10} &= 16.028.674003 \\
 a_{11} &= -5354.1038967 \\
 a_{12} &= 1199.031906 \\
 a_{13} &= -161.46362959 \\
 a_{14} &= 9.8811553386
 \end{aligned}$$

The other liquid helium properties were obtained from 12 point orthogonal polynomial least squares curve fits of values given in Donnelly, Experimental Superfluidity, 1967. The values used are given in Table V. The density of the super fluid,  $\rho_s$ , and the total density,  $\rho$ , are obtained from the values of  $\rho_n$  and the ratio of  $\rho_n$  to  $\rho$  given in the table. Therefore,

$$\rho_s = \rho_n / (\rho_n/\rho) - \rho_n \quad (43)$$

Table V: Liquid Helium Properties

T	S	L	$\rho_n$	$\rho_n/\rho$	$\mu$
Temperature	Entropy	Latent Heat of Vaporization	Normal Fluid Density	Ratio of Normal to Total Fluid Density	Viscosity of Normal Fluid Micro-poise
$^{\circ}\text{K}$	$\text{j/gm}^{\circ}\text{K}$	$\text{cal/mole}$	$\text{gm/cm}^3$		
1.1	.0304	19.75	.00212	.0146	26.8
1.2	.0523	20.30	.00405	.0279	17.5
1.3	.0853	20.80	.00686	.0473	15.2
1.4	.132	21.20	.01100	.0743	14.1
1.5	.197	21.48	.01650	.1140	13.5
1.6	.284	21.78	.02465	.1700	13.2
1.7	.398	22.05	.03460	.2380	13.0
1.8	.535	22.20	.04720	.3250	13.0
1.9	.709	22.26	.06240	.4290	13.4
2.0	.929	22.18	.08070	.5540	14.9
2.1	1.215	22.02	.10550	.7230	18.6
2.2	1.600	21.87	.14600	1.000	28.0

and

$$\rho = \rho_s + \rho_n \quad (44)$$

### Thermal Conductivity

Values of the thermal conductivity of the plug materials were obtained from National Bureau of Standards, NBS Monograph 131, Thermal Conductivity of Solids at Room Temperature and Below, 1973. At the temperatures under consideration, the material thermal conductivities are found to vary in a linear manner on a log-log plot of conductivity and temperature. The thermal conductivity is then written as

$$K_m = \text{EXP} (A + B \log T) \quad (45)$$

where A and B are the parameters of the straight line curve fit.

Thermal conductivity is found to be a strong function of the impurities or the alloy of the material under consideration. Table VI gives a sampling of the thermal conductivities of various materials at 2°K. Figure 1 shows the variation of thermal conductivity with respect to temperature for a number of materials.

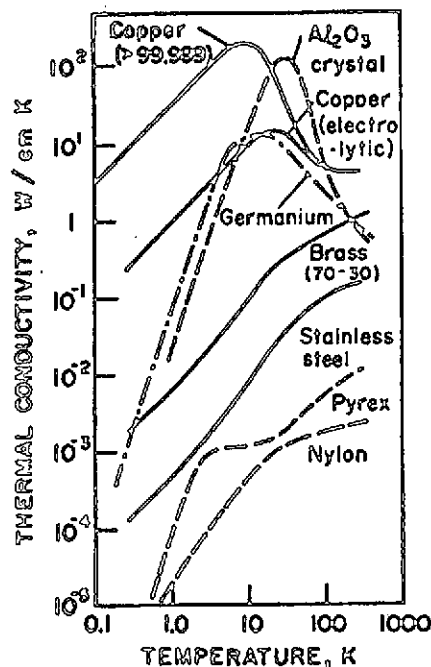


Figure 1:

Thermal conductivity variations of metals and alloys (—), electrical insulators (---), and a semi-conductor (o—o—).

Table VI: Thermal Conductivity of Materials at 2°K

Material		$K_m$ (W/m · °K)
Nickel	-high purity RRR = 670	550.0
	-Matthey 37043, 99.995 pure	47.5
	-.16 atomic percent Cu	20.0
Silver	-better than 99.99% pure	370.0
Gold	-99.999% pure with traces of Cu, Ag, Si, and Pb. RRR = 536	125.0
Copper	-.003% Ag, Ni, and Pb	118.0
	-Commercial wire RRR $\approx$ 85	260.0
Stainless Steel	-Extrapolation of Mean of number of stainless steels	$\approx$ 0.10
Alumina $Al_2O_3$	-Sintered to within 5% of crystal density, extrapolated value	$\approx$ .3
	-Doped with .1 (weight) $M_n O_2$	13.5
Fused Quartz-Extrapolated from 100°K		$\approx$ .08
Aluminum	-99.998% pure	480.0
	-Alloys (extrapolated)	$\approx$ 2.0
Titanium	-99.99% pure	$\approx$ 1.0
	-98 % pure	$\approx$ .4

For comparison, Table VII gives the effective thermal conductivity of liquid helium at 2°K calculated using Equation 19.

Table VII: Thermal Conductivity of Liquid Helium at 2°K (Equation 19)

Pore Size (microns) of flow passage	$K_L$ W/m °K
0.1	20.46
0.5	511.54
1.0	2,046.2
5.0	51,154.0
10.0	204,620.0

The thermal conductivity of the liquid is seen to be generally higher than the material values given in Table VI except for pore sizes less than .5 micron in diameter.

The thermal conductivities of the porous plug materials are expected to be less than the bulk material because of the granular structure of the plug. Since thermal conductivity measurements were not made of the porous materials used in the plug tests, the bulk properties are employed in the analysis with the realization that these conductivities are likely higher than that of the porous material. The error made in using the higher conductivity values is not important for large pore plugs since the liquid helium thermal conductivity dominates the total conductivity. For cases in which the conductivity of the plug material is important (for pore sizes less than 0.5 micron), better values of thermal conductivity are needed in order to accurately predict the plug operation. While the relationships used here are expected to be in error in absolute value, the variation with respect to temperature is represented. The characteristics of small-pore-size plugs revealed in experiments may yield improved values of thermal conductivity when such results are compared with those predicted.

In view of the lack of porous material conductivity information as discussed above, curve fit parameters A and B were derived to represent a number of different materials. These values are given in Table VIII.

Table VIII: Curve Fit Parameters for Thermal Conductivity\*

Material Represented	A	B	$K_m (2^\circ K), W/m^\circ K$
Nickel - high purity	-.17712	.78873	144.7135
Aluminum Alloy	-4.8655	1.0269	1.5706
Copper	.2332	1.008	253.93
Alumina ( $Al_2 O_3$ )	-3.141	1.348	11.
Beryllium Oxide ( $BeO$ )	-9.388	2.817	.059
Stainless Steel	-.8011	1.239	105.94
Quartz	-8.087	.8472	.055

\*Values of A and B listed here, when used in Equation 45, will give thermal conductivity in units of  $W/cm^\circ K$ .

#### Area of Pores, $A_p$ , and Area of Material, $A_m$

The effective area available for flow of liquid helium is obtained in the following derivation. Let the flow passages for the liquid helium be approximated by straight tubes of constant diameter. If each tube were to have the diameter of the pore size of the plug, then each tube would have an empty volume of

$$\text{Volume of one flow tube} = \pi \left( \frac{d}{2} \right)^2 \ell \quad (46)$$

If it is assumed that the flow tubes comprise all of the empty space of the plug, the total volume of voids,  $V_v$ , is

$$V_v = N \pi \left( \frac{d}{2} \right)^2 \ell \quad (47)$$

where  $N$  is the number of flow tubes. The value of  $N$  for a particular plug is found from the porosity measurements as follows. Since porosity is defined as

$$P = \frac{V_v}{V_b} \quad (48)$$

where  $V_b$  is the bulk volume of the plug. The value of  $N$  is then found from Equations 47 and 48

$$N = \frac{P V_b}{\pi \left( \frac{d}{2} \right)^2 \ell} \quad (49)$$

The total area of pores is found to be

$$A_p = N \pi \left( \frac{d}{2} \right)^2 = \frac{P V_b}{\ell} = \frac{P A_T \ell}{\ell} \quad (50)$$

The following expressions are therefore obtained

$$A_p = P A_T \quad (51)$$

and

$$A_M = A_T - A_p = (1-P) A_T \quad (52)$$

These estimates of  $A_p$  and  $A_T$  will be employed in the relationships describing the liquid helium flow in porous materials.

### Pore Size Estimation

The size of the pores in the porous plugs tested are not uniform as evidenced by electron microscope pictures made of a number of the plugs. The labeled values of pore size are very approximate and is meant as only an estimate of the pore size. Since pore size is required in the evaluation of the equations presented here, it was decided to relate the pore size to the measured value of permeability rather than use the labeled value.

The permeability measurements given in Table III were least squares fit with respect to the labeled pore size. A linear curve fit was employed with the result

$$d = (\Delta F / \Delta P) / 2.5 \quad (53)$$

where  $d$  is the pore diameter (assumed to have a circular cross section) and  $\Delta F / \Delta P$  corresponds to the room temperature helium gas flow given in Table III in units of standard cubic centimeters per second per psi of pressure drop (SCC/SEC/psi). The value of  $d$  determined using Equation 46 will be given in units of microns.

### Results

The above relationships were evaluated on the UAH Univac 1108 computer. The computations were performed using the international system of units. The flow rates were then converted to units of Standard Cubic Centimeters per Minute (SCC/M) for ready comparison with the experimental measurements which were made in those units. Table IX gives the results for the first plug tested which was nickel having the properties listed with the table. Table X gives results of the 10 micron ceramic and Table XI gives results for .5 micron ceramic.



Table IX: Results for Nickel Plug (10 Micron)

Material = Nickel

Porosity = .38411

Pore Size = 12.58

Thickness = .0063 m

Thermal Conductivity at 2<sup>o</sup>K = 144 W/m<sup>o</sup>KPermeability =  $3.77 \times 10^{-13} \text{ m}^2$ 

Temperature <sup>o</sup> K	Flow Rate SCC/M	$V_n$ m/sec	$V_s$ m/sec
1.1	20.3	$.538 \times 10^{-5}$	$.653 \times 10^{-6}$
1.2	43.6	$.116 \times 10^{-4}$	$.127 \times 10^{-5}$
1.3	84.4	$.152 \times 10^{-4}$	$.237 \times 10^{-5}$
1.4	150.7	$.176 \times 10^{-4}$	$.432 \times 10^{-5}$
1.5	251.7	$.191 \times 10^{-4}$	$.761 \times 10^{-5}$
1.6	398.1	$.201 \times 10^{-4}$	$.130 \times 10^{-4}$
1.7	601.0	$.208 \times 10^{-4}$	$.216 \times 10^{-4}$
1.8	872.3	$.213 \times 10^{-4}$	$.356 \times 10^{-4}$
1.9	1,223.3	$.214 \times 10^{-4}$	$.599 \times 10^{-4}$
2.0	1,663.8	$.210 \times 10^{-4}$	$.106 \times 10^{-3}$
2.1	2,200.0	$.201 \times 10^{-4}$	$.229 \times 10^{-3}$
2.16	2,568.0	$.192 \times 10^{-4}$	$.563 \times 10^{-3}$

Table X: Results for Ceramic Plug (10 micron)

Material = Ceramic

Porosity = .677

Pore Size = 7.456 micron

Thickness = .0066 m

Thermal Conductivity at 2°K = 11 W/m °K

Permeability =  $2.2354 \times 10^{-13} \text{ m}^2$ 

Temperature °K	Flow Rate SCC/M	$V_n$ m/sec	$V_s$ m/sec
1.1	20.0	$.113 \times 10^{-4}$	$.241 \times 10^{-6}$
1.2	43.4	$.142 \times 10^{-4}$	$.496 \times 10^{-6}$
1.3	84.2	$.158 \times 10^{-4}$	$.986 \times 10^{-6}$
1.4	150.5	$.174 \times 10^{-4}$	$.185 \times 10^{-5}$
1.5	251.6	$.186 \times 10^{-4}$	$.332 \times 10^{-5}$
1.6	397.9	$.194 \times 10^{-4}$	$.573 \times 10^{-5}$
1.7	600.8	$.200 \times 10^{-4}$	$.966 \times 10^{-5}$
1.8	872.1	$.204 \times 10^{-4}$	$.162 \times 10^{-4}$
1.9	1,223.0	$.205 \times 10^{-4}$	$.277 \times 10^{-4}$
2.0	1,663.6	$.202 \times 10^{-4}$	$.500 \times 10^{-4}$
2.1	2,199.7	$.192 \times 10^{-4}$	$.109 \times 10^{-3}$
2.16	2,567.7	$.184 \times 10^{-4}$	$.270 \times 10^{-3}$

Table XI: Results for Ceramic Plug (.5 micron)

Material = Ceramic

Porosity = .548

Pore Size = .1792 micron

Thickness = .0065 m

Thermal Conductivity at 2°K = 11 W/m °K

Permeability =  $5.3726 \times 10^{-15} \text{ m}^2$

Temperature °K	Flow Rate SCC/M	$V_n$ m/sec	$V_s$ m/sec
1.1	16.0	$.260 \times 10^{-5}$	$.366 \times 10^{-6}$
1.2	30.7	$.117 \times 10^{-4}$	$.455 \times 10^{-6}$
1.3	52.2	$.336 \times 10^{-3}$	$-.304 \times 10^{-6}$
1.4	83.9	$.747 \times 10^{-4}$	$-.377 \times 10^{-5}$
1.5	130.9	$.141 \times 10^{-3}$	$-.146 \times 10^{-4}$
1.6	204.5	$.231 \times 10^{-3}$	$-.409 \times 10^{-4}$
1.7	321.7	$.338 \times 10^{-3}$	$-.954 \times 10^{-4}$
1.8	502.7	$.448 \times 10^{-3}$	$-.197 \times 10^{-3}$
1.9	761.3	$.543 \times 10^{-3}$	$-.374 \times 10^{-3}$
2.0	1,096.1	$.600 \times 10^{-3}$	$-.685 \times 10^{-3}$
2.1	1,484.9	$.606 \times 10^{-3}$	$-.145 \times 10^{-2}$
2.16	1,717.4	$.580 \times 10^{-3}$	$-.351 \times 10^{-2}$

### Discussion of Results

While a large number of tables could be generated, the three tables of results provided here are sufficient to illustrate many of the basic characteristics of all the results obtained using the relationships provided.

#### a. Comparison with experiment

Table XII gives samples of the results obtained in experiments conducted at MSFC and Stanford.

Table XII: Experimental Results

Temperature	MSFC Nickel Plug 7 - 10 micron SCC/M	Stanford Rolled Aluminum Foil Plug SCC/M
1.6	370.	312.
1.7	540.	564.
1.8	760.	803.
1.9	1200.	624.
2.0	1900.	442.
2.1	3000.	336.
2.16	3800.	336.

The Stanford results were obtained from "Research at Stanford on the Containment of Liquid Helium in Space by a Porous Plug and a Long Hold-Time Dewar for the Gyro Relativity Experiment" by Lipa, Everitt, and Fairbank. The fact that the MSFC plug and the Stanford plug had different dimensions was not taken into consideration in constructing Table XII.

The experimental results given in Table XII show similar total flow rates in the range of 1.6 °K to 1.8 °K for both the MSFC and Stanford plugs. However, at 1.8 °K and higher, the Stanford plug shows a reduction in flow rate with increasing temperature to the lambda point. The MSFC plug on the other hand shows a monotonically increasing flow rate with increasing temperature which is in agreement with that predicted by the equations developed here as given in Tables IX, X, and XI.

The theory developed here is found to predict the behavior of the MSFC large pore Nickel plug with respect to temperature. While the shape of the flow rate versus temperature curve is accurately predicted, the values predicted are about 30% less than that measured at temperatures near the lambda point. The agreement at lower temperatures is progressively better until the best agreement is reached at 1.6 °K. (7.5% error).

The reason the theory has such large error at the higher temperatures was traced to the value of the pumping factor  $\frac{FA^*}{A}$  used in the program. This factor was determined for flow measurements made near 1.6 °K. If the pumping line restriction were an ideal choked orifice as modeled, this factor would be constant. However, since the restriction is more complex, the factor is not constant and is found to increase as the pressure on the gas side of the plug increases. Future work will modify the model of the pumping line restriction to yield improved comparison with experiment.

ORIGINAL PAGE IS  
OF POOR QUALITY

FINANCIAL STATUS REPORT

Contract No. NAS8-29316

- I. Expenditures to date as of June 30, 1974 beginning with the UAH  
fiscal year October 1, 1973 and each previous year, if any. \$102,326.54
- II. Forecast of funds required for completion: 61,914.46
- III. Problem areas:

ORIGINAL PAGE IS  
OF POOR QUALITY